Chemistry and Materials Research
ISSN 2224- 3224 (Print) ISSN 2225- 0956 (Online)
Vol.6 No.9, 2014

Adsorptive Power Evaluation of the Nano-Crystalline Mo-W Bimetallic Oxides

Heba H. El-Maghrabi*, Sara Mikhail, Tamer Zaki

Department of Catalysis, Petroleum Refining Division, Egyptian Petroleum Research Institute, 11727, Cairo, Arabic Republic of Egypt
* E-mail of the corresponding author: hebachem@yahoo.com

Abstract

Novel nanosized molybdenum-tungsten bimetallic oxides were prepared by modified Pechini method based on the low temperature polymerization-complexation steps. The physical properties of the prepared nanoparticles were characterized by: X-ray diffraction (XRD), Fourier transformer inferred spectroscopy (FT-IR), differential thermal analyses (DCS), and high resolution transmission electron microscopy (HRTEM). The influence of metal molar ratios (Mo/W) on the morphology and the crystallization the samples was also investigated. The adsorptive power of prepared samples was evaluated through the removal of dimethyl disulfide sulfur compound (in cyclohexane as fuel). The results indicate that all the prepared Mo-W oxide materials are nanoparticles with diameter ranging between 1 and 70 nm. And the smallest nanosize particles enhanced the adsorptive power of the prepared nanostructured Mo-W bimetallic oxide.

Keywords : Mixed Oxide, Synthesis, Characterization, Sulfur Adsorption.

1. Introduction

Sulfur and nitrogen based compounds are nonhydrocarbon species typically found in the petroleum oil with considerable percents. These species seriously pollute the environment whereas SO*x* and NO*x* are virtually the ends of their degradations [Babich and Moulijn, 2003]. In addition, they are poisons for catalysts used in automobile vehicles, e.g., group VIII metal catalysts [Whitehurst et. al., 1998]. The sulfur content in gasoline for example when used as a feed for fuel cell applications must be reduced to less than 0.1 ppmw to avoid catalyst poisoning [Ma et. al., 2005]. As a result, a growing of the stringent environmental legislations against these species could be seen spread all over the world [US EPA, 1999]. Due to the wide broad applications and the increasing demand for the petroleum oil distillates, the refining industry has put removing such species as one of their top priority issues. Hydrodesulfurization is by far the top leading process to achieve this target. The target on obtaining a fuel with ultra-low or even free sulfur is still far to be attained in a large economic scale [Babich and Moulijn, 2003].
Several technologies are pointed out and proposed as partials and/or alternatives to hydrodesulfurization. Among these technologies are: (a) desulfurization based on a bio-catalytic process in which a genetically engineered bacteria converts the sulfur in the petroleum products to sulfates [Prince and Grossman, 2003]. (b) The oxidative desulfurization of sulfur containing compounds using oxidizing agents (hydrogen peroxide for example) followed by separation of the readily oxidized sulfur compounds [Te et. al., 2001] and (c) The selective reactive adsorption of sulfur compounds. This can further be subdivided onto two classes, depending on the affinity of linkages that bind the adsorbate with the adsorbent active sites, adsorption via chemical interactions, and adsorption via physical interactions.
The research on the selective adsorption removal of sulfur compounds from the petroleum oil distillates seems to be attractive; however, it is still in its preliminary stages. Selective adsorption removal of the sulfur compounds could prove its economic feasibility and efficiency at the industrial level. It could rather be promise for further development and improvement.

The challenge is to find a proper sorbent with high capacity and selectivity toward the sulfur compound and to be regenerable. In the present study, the main trend of this work is the preparation of crystalline nano-sized particles Mo-W bimetallic oxides [Hassan et al., 2012], and the availability of these materials to be used as adsorbents for removing the sulfur compounds from the petroleum fraction. The precursors and the prepared materials have been characterized by applying different techniques; thermal heating, degree of crystallization, surface morphology and particle size via DSC, XRD, FTIR and TEM analyses.

2. Experimental

Aqueous ethylene glycol (EG) solution was added to an aqueous solution of citric acid (CA) to carry out the polymerization reaction at 60 ℃ under constant stirring for one hour [Pechini, 1967& Zaki et al., 2012]. The reaction temperature was elevated to 80 ℃ and 500 mL TM solution of Mo/W (ammonium heptamolybdate / ammonium metatungstate precursors) with 1:1 metal ratio was added during the stirring for an additional hour. Accordingly, the molybdic and the tungstic acids were produced, and then the products were subjected to heating to 140 ℃ until the water was completely evaporated (~2.5 hours). The obtained gel was dried at 150 ℃ overnight to form the solid resin. The resulting resin was ground in an agate mortar and subjected to a pyrolysis process at 450 ℃ for 4 hs. Finally, the pyrolyzed product was subjected to calcination at 500 ℃ for 4 h in the presence of purified air. The produced samples were named MxWR_C-R_E (x is Mo:W ratios, R_C is CA:TM = 2, and R_E is EG:CA=1.5).

The structural and morphology of the prepared samples have been studied by different techniques; X-ray analysis to study the crystalline structure, differential thermal analyses to trace the structural changes that take place during the thermal heating, Transmission electron microscopy (TEM) to investigate the morphology and the size distribution of the nanoparticles and FTIR spectra to characterize the main constituents of the prepared samples.

Adsorption reaction of dimethyl disulfide sulfur compound was performed using the prepared Mo-W oxides nanoparticles materials in a batch technique.

Adsorption experiments were investigated at an ambient temperature by a batch technique. In all experiments 0.1 gm of the prepared adsorbent material was placed in a bottle flask (50mL capacity), the required volume (10 mL, C^0 = 50 mg L^{-1}) of dimethyl disulfide solution (dissolved in cyclohexane) was added and the suspension was magnetically stirred for a given time period to reach equilibrium. After completion of a pre-selected contact time, the suspension was then filtered. The bimetallic oxide sample was suffered to different contact time in the range of 5–120 min, in order to gain understanding about the time-dependent behavior of sulfur. Also the adsorptive volume (dimethyl disulfide cyclohexane solution) was varied from 10 to 50 ml at constant agitation time of 60 min. The amount adsorbed was determined by analyzing the total sulfur before and after each experimental using X-ray florescence analysis on a LAB apparatus.

3. Results and Discussion

3.1 Characterizations of the prepared molybdenum-tungsten bimetallic oxides samples

3.1.1 X-ray diffraction analysis

The X-ray diffraction patterns (Fig. 1) for the prepared materials M0.2W2-1.5 → M0.8W2-1.5 reveal the appearance of $W_{0.71}Mo_{0.29}O_3$ phase, (JCPD:76-1279) for the sample M0.2W2-1.5, in which tungsten oxide is the major component. With the increase in Mo/W ratio "sample M0.4W2-1.5" deformation of bimetallic phases happened. For sample MW2-1.5 (Mo/W ratio = unity) the reflection lines emphasized the appearance of the only phase $Mo_{0.5}W_{0.5}O_3$. Further, increasing in Mo for samples M0.6W2-1.5 and M0.8W2-1.5 the crystallinity of molybdenum oxide phases; monoclinic MoO_3 (JCPD:47-1320) and orthorhombic MoO_3 (JCPD:05-0508), is sharply increased.

For samples M2-1.5 and W2-1.5, complete separation between the two metal oxides occurred. The diffractogram for sample, W2-1.5, reveals the presence of the only triclinic WO_3 phase (JCPD:83-0948) (Fig. 1). Meanwhile, the X-ray diffraction pattern for the sample M2-1.5 reveals that the sample consisted of monoclinic MoO_3 (JCPD:47-1320) and orthorhombic MoO_3 (JCPD:05-0508) phases accompanied with a high crystallinity.

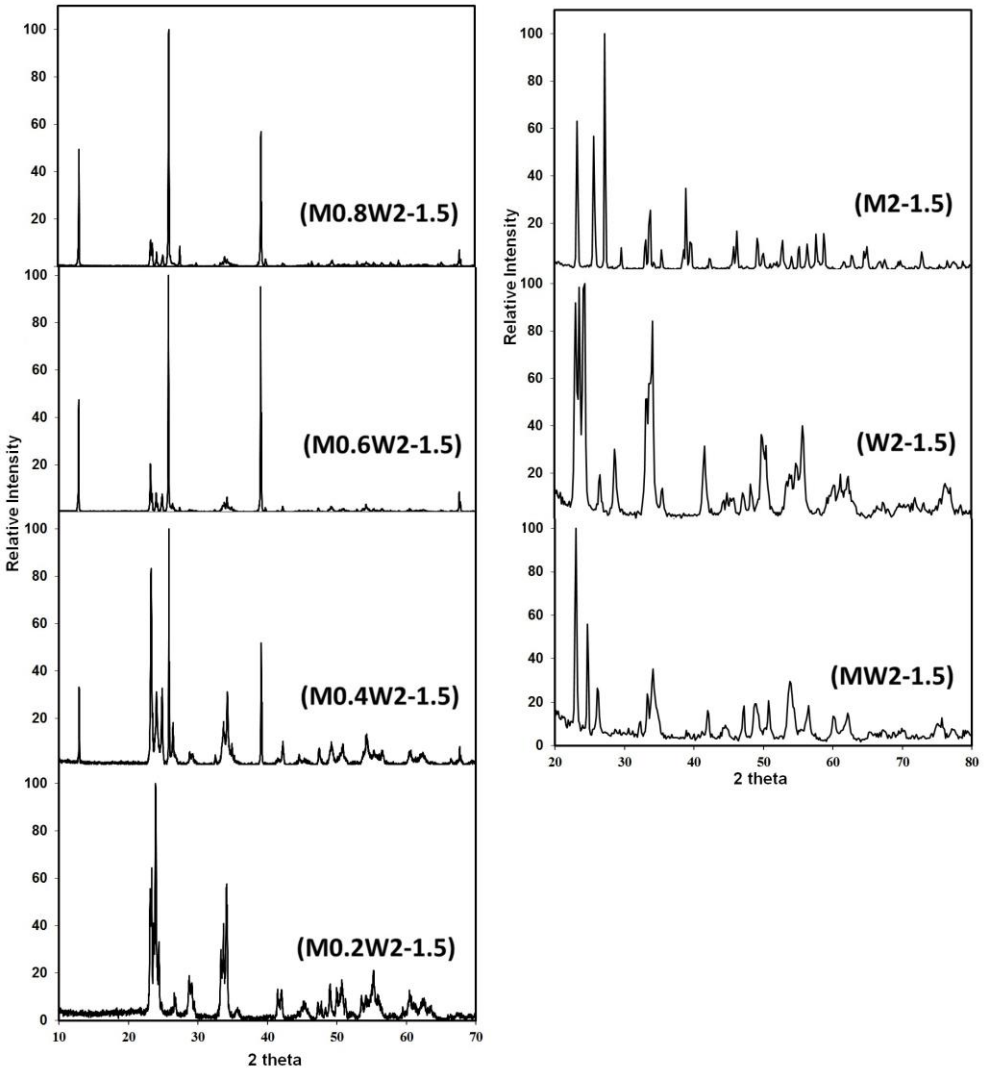

Figure 1. X-ray diffraction patterns for Mo-W oxide samples with different Mo/W ratios.

3.1.2 Transmission electron microscopy (TEM)

TEM images (Fig. 2) for the samples M2-1.5, M0.6W2-1.5, M0.8W2-1.5 and M0.4W2-1.5 show that the shape of the particles is mostly square and their particle sizes are almost uniform. They also signify that the average particle sizes increases from 11-16 nm to 27-40 nm with the gradual decrease in Mo/W ratios except for sample W2-1.5 where the tungsten metal is major, the average particle size slightly decreases as represented histogramtically in Fig. 3.

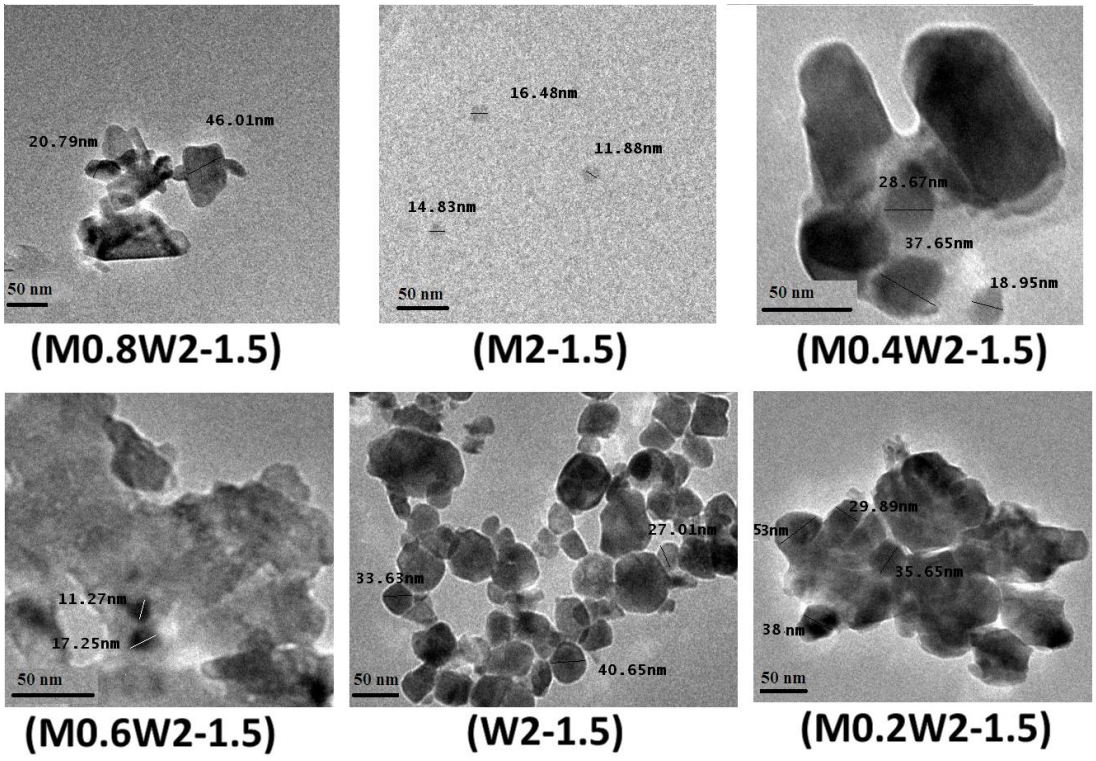

Figure 2. TEM images for Mo-W oxide samples with different Mo/W ratios.

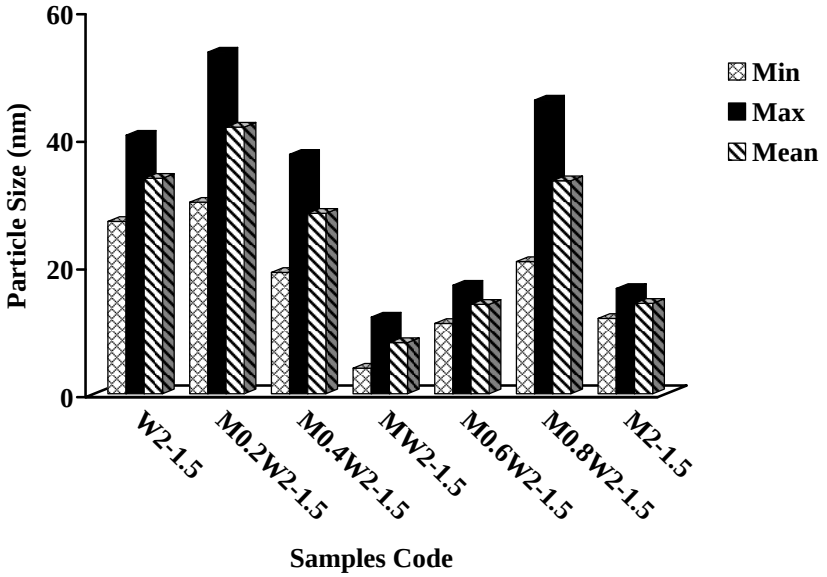

Figure 3. Particle size range for the Mo-W oxide samples with different Mo/W ratios.

3.1.3 Fourier transformer inferred spectroscopy (FT-IR)

FT-IR spectra of MW2-1.5 and W2-1.5 samples are represented in Fig. (4). The FT-IR spectrum of MW2-1.5 shows a broad band located in the range of 500-1000 cm^{-1}, which has distinguishable apexes at 633, 767 and 845 cm^{-1} (Fig. 4a). The bands at 633 and 845 cm^{-1} are attributed to the asymmetric and symmetric stretches of W–O–W bridges, respectively [V. Tolstoy et al., 2003]. The band appeared at 767 cm^{-1} which assigned to Mo–O–W stretching [Zhu et. al., 2008].

The spectrum of the prepared W2-1.5 sample shows a broad band which is ascribed into two apexes at 633 and 845 cm^{-1} (Fig. 4b) distinguish a narrowing in this peak due to the absence of the bands related to the vibration of the Mo–O–Mo bond at 882 cm^{-1} [Sarkar et al., 2008] in agreement with x-ray diffraction analyses.

Moreover, a new shoulder band appeared at 1040 cm^{-1} attributed to the stretching of W–O bonds at the surface [J. Yu et al., 2008].

The FT-IR spectrum of the needled sample, M2-1.5, (Fig. 5) reveals the appearance of orthorhombic MoO_3, which has two significant bands assigned at 975 cm^{-1} for a terminal Mo=O stretching vibration, and at 840 cm^{-1} for the vibration of the Mo–O–Mo species [V. Tolstoy et al., 2003]. Bands at 492 and 533 cm^{-1} assigned to the asymmetric and symmetric stretches of the monoclinic MoO_3 phase. The bands at 1625 and 3430 cm^{-1} can be assigned to the H–O–H bending and stretching vibrations of the hydrated water [S. Wang et al., 2006].

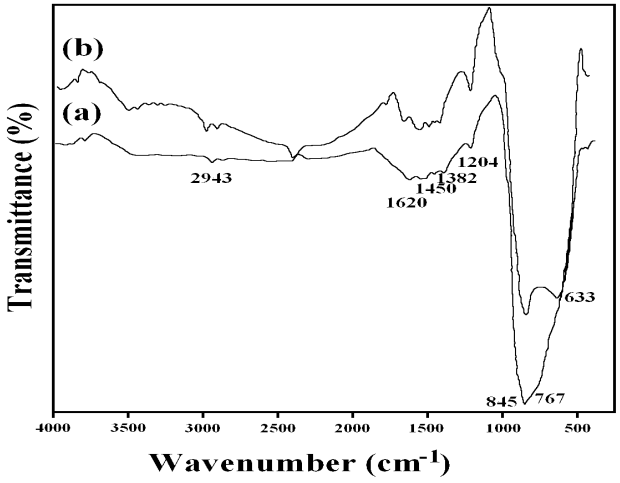

Figure 4. FTIR spectra of (a) MW2-1.5 and (b) W2-1.5 samples.

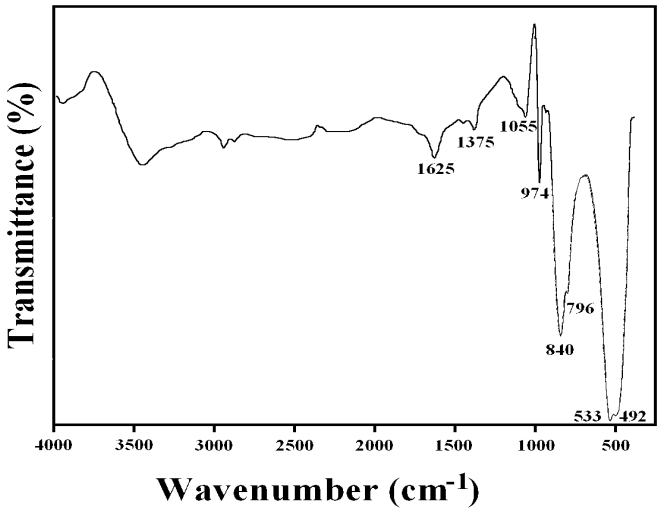

Figure 5. FTIR spectrum for M2-1.5 sample.

3.1.4 Differential Thermal Analyses

From the previous results, the x-ray diffraction analysis and FT-IR spectra clarified that the decomposition of the bimetallic nanoparticles and, consequently, the sublimation process started early at ≈ 700°C. On the contrary, earlier published data [El-Shobaky et al., 1999] demonstrated that the molybdenum oxide (MoO_3) melts and sublimes at approximately 800 ℃. As regarded to the thermal analysis of sample MW2-1.5 (Fig. 6), where the

thermal profile of the MoW nanoparticles represents a strong decline in the curve towards the endothermic direction at the temperatures range 600-950 ℃ with two endothermic peaks centered at 880 and 933 ℃.

The thermal behavior of the MW2-1.5 sample may be explained as follows:

- Between 700 and 800 ℃, the decomposition and deformation of the $Mo_{0.5}W_{0.5}O_3$ phase occurred (confirmed by x-ray analysis), as did sublimation of the free MoO_3 particles.
- The sublimation of the free MoO_3 at such a relatively low temperature with respect to the normal thermal behavior of the molybdenum oxide bulk phase [W.M. Shaheen, 2002] might be due to its nanoparticle size.
- On a nano-scale, the particles are more sensitive to thermal changes and consequently, the thermal transformation process become easier than that for the bulky particles.
- With the temperature range 800 - 900 ℃, the $W_{0.47}Mo_{0.53}O_3$ and $W_{0.4}Mo_{0.6}O_3$ phases deformed into $W_{0.71}Mo_{0.29}O_3$. Which accompanied by sublimation of the produced free MoO_3 phase.
- At 933 ℃, the final form of the MoW nanoparticles, $W_{0.71}Mo_{0.29}O_3$, lost its molybdenum component and transformed into triclinic WO_3.

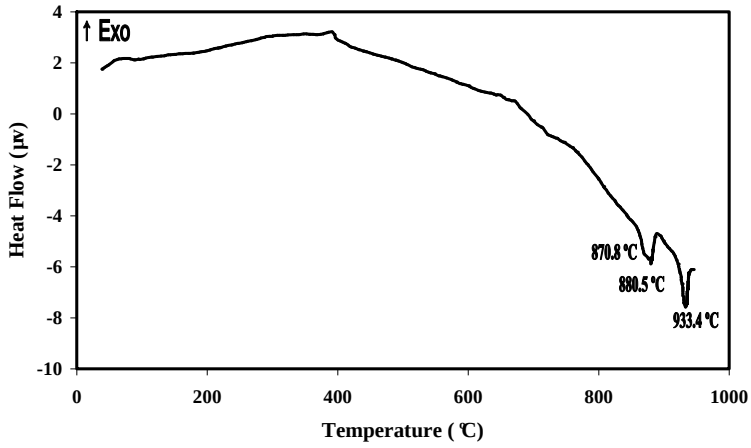

Figure 6. Thermal analysis profile (DSC) for the prepared MW2-1.5 sample.

3.2 Evaluation of the prepared nanosized molybdenum-tungsten bimetallic oxides as adsorbents

Dimethyldisulfide solution was chosen as an adsorbate compound to evaluate the efficiency of the prepared nanosized molybdenum-tungsten bimetallic oxides towards sulfur removal via adsorbtion under variables experimental conditions. Data are graphically illustrated in figures (7→15).

3.2.1 Effect of the Mo/W ratio

The nature of the adsorbent was varied according to the different sites that constituting the prepared Mo-W oxide powders with the variation in Mo/W ratio. In all adsorption experiments throughout this investigation: 73.5 ppm initial concentration of dimethyldisulfide in cyclohexane, agitation time of 30 min and amount of adsorbent 100 mg on using the prepared Mo-W oxide powders with Mo/W ratio ranged from 0/1 to 1/0 were used.

Histogram in Figure (7) represents the relation between the increase in Mo/W ratio and the specific adsorption of DMDS per gm of the adsorbent powder.

Results show that the sample MW2-1.5 (Mo/W = 0.5/0.5) was the most active adsorbent (highest adsorption %) as compared with the other samples as Mo/W ranged from 0/1 to 1/0.

The higher adsorption capacity for such sample attributed to the smallest nanoparticles sizes of the Mo0.5W0.5O3 phase (the only phase in MW2-1.5 sample as confirmed by XRD Fig. 1). This nano-sized particles create active sites as it is well distributed as clarified from TEM image (Fig 2), i.e. arising homogeneous active adsorbent sites, able to remove the sulfur heteroatoms and consequently strongly contribute to sulfur compound removal. Meanwhile, the samples M0.2W2-1.5, M0.4W2-1.5, M0.6W2-1.5 and M0.8W2-1.5 contain the monoclinic MoO3 and the orthorhombic WO3 phases the powdered sample (W2-1.5) contains only a triclinic WO3 and the powdered sample (M2-1.5) contains only a monoclinic MoO3, in addition to the major phase Mo0.5W0.5O3 (X-ray data Fig. 1).

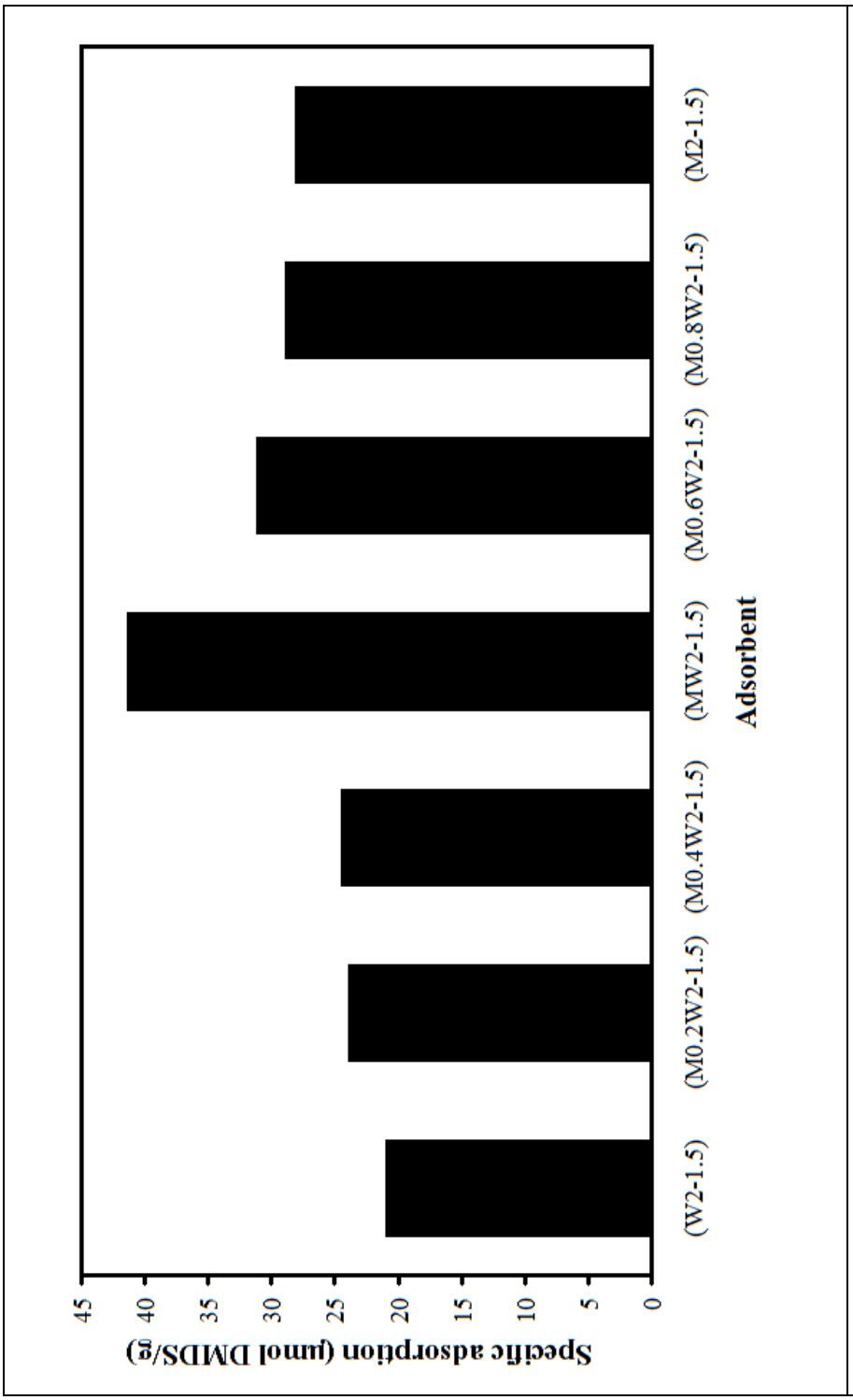

Figure 7. effect of Mo/W ratio of the prepared samples on the specific adsorption %.

3.2.2 Effect of the contact time

From the above results it can be decided that the prepared MW2-1.5 nanoparticles is the best adsorbent material.

The time-dependent behavior of sulfur adsorption was measured by varying the equilibrium time between the adsorbate and the adsorbent in the range of 5–120 min (Fig. 8). The initial concentration of DMDS was 73.5 ppm and the amount of adsorbent was 100 mg.

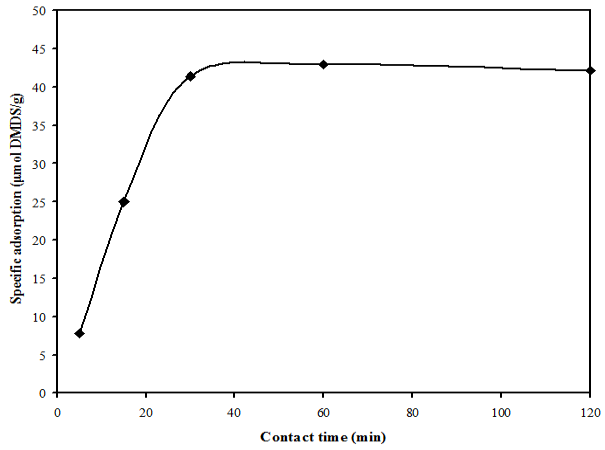

Figure 8. The relation between the specific adsorption and contact time.

Data in fig (8) show that the equilibrium reached quickly after 30 min, which indicates that the adsorption sites are well exposed. With the increase in contact time from 30 to 60 min the adsorbed amount are slightly increased followed by a constant adsorption upon further increasing in contact time. Consequently, the contact time was fixed at 60 min for the rest of the batch experiments to ensure that the adsorption equilibrium was reached in each case.

3.2.3 Effect of the amount of adsorbent

The amount of adsorbent was varied from 100 to 300 mg with an initial DMDS concentration of 73.5 mg/l and an agitation time 60 min. The extent of adsorption shows a gradual increase as the amount of the adsorbent material increases from 100 to 300 mg (the adsorption %increases from 53 to 65 % successively Fig 9). The up-taking enhancement may be attributed to the increase in the available number of adsorption sites.

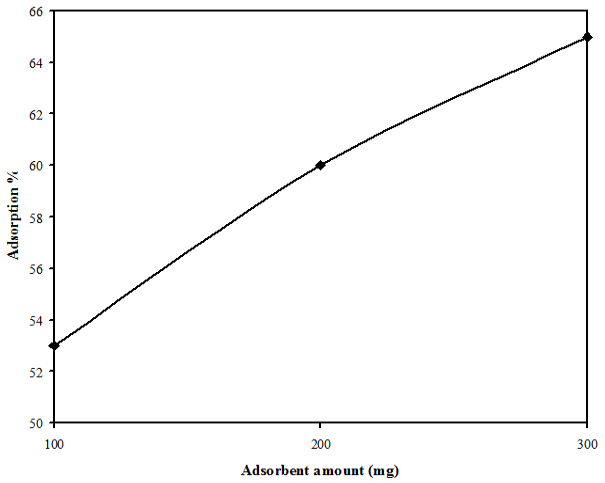

Figure 9. Relation between adsorbent amount and adsorption %.

3.2.4 Effect of the adsorptive sulfur volume

When the adsorptive volume of sulfur was changed from 10, 20, 30, 40 to 50 mL on using 100 mg of the adsorbent, initial sulfur concentration 73.5 ppm and agitation time 60 min, the extent of the specific adsorption of DMDS per gm of the adsorbent materials slightly increases with the gradual increase in the initial DMDS adsorptive volume (Fig 10). Such observation is quite common.

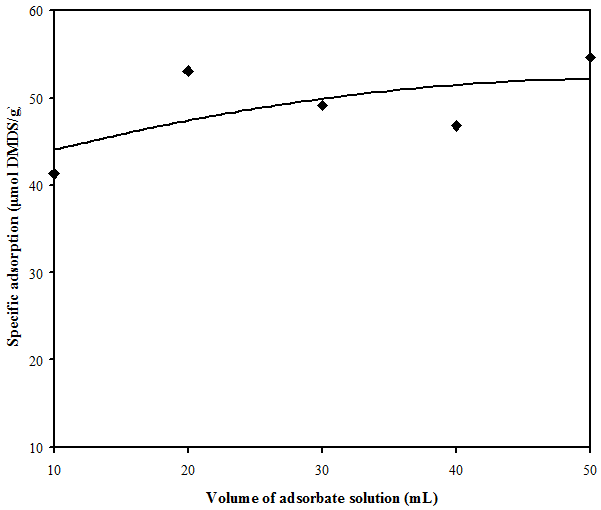

Figure 10. Effect of adsorptive volume on the specific adsorption of DMDS.

3.2.5 Effect of the initial DMDS concentration

When the initial concentration of sulfur was changed from 0.16, 0.31, 0.47, 0.62 and 0.78 mmol/L on using 100 mg of the adsorbent, agitation time 60 min and 10 mL of the adsorptive DMDS, the extent of adsorption gradually increases with the gradual increase in the initial DMDS concentration from 0.16 to 0.78.

As indicated from the equilibrium adsorption data (fig. 8) the sorption capacity of the prepared nanoparticles MW2-1.5 sample reached 41.33 µmol/g.

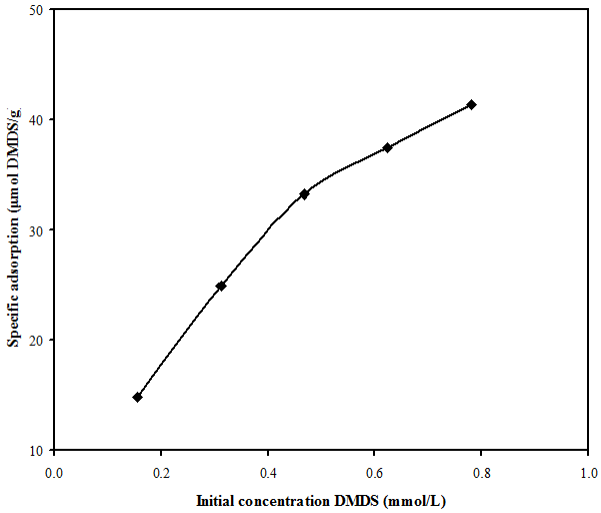

Figure 11. Effect of initial sulfur concentration on the specific adsorption of DMDS.

The equilibrium characterization of the adsorptive desulfurization process was investigated by fitting the experimental data to Langmuir and Freundlich isotherms.

The equilibrium expression of the Langmuir model is:

$$q = Q_m [(K_L . C_e)/(1+(K_L . C_e))] \quad (1)$$

where C_e (mmol/L) denotes the equilibrium concentration of sulfur in adsorptive solution, K_L (L/mmol) represents the Langmuir constant that relates to the affinity of binding sites and Q_m (mmol/g) is the theoretical capacity of the monolayer. The linear form of Eq. (1) is as follows:

$$(C_e/q) = [1/(Q_m.K_L)] + (C_e/Q_m) \quad (2)$$

The values of K_L and Q_m are calculated from the intercept and slope of the linear plot of (C_e/q) versus C_e.

In addition, the separation factor, R_L, or equilibrium parameter was calculated from the following expression:

$$R_L = 1/[1 + (K_L.C_0)] \quad (3)$$

where C_0 (mmol/L) is the initial DMDS concentration. Separation factor can be used for evaluating the adequacy of adsorption process, i.e. when $0 < R_L < 1$ adsorption is favorable, $R_L > 1$ adsorption is unfavorable, $R_L = 1$ adsorption is linear and $R_L = 0$ adsorption is irreversible.

The Freundlich isotherm is represented by an empirical model that assumes heterogeneous adsorption due to the diversity of adsorption sites and has the following form:

$$q = K_F.(C_e)^{(1/n)} \quad (4)$$

where K_F and n are equilibrium constants indicative of adsorption capacity and adsorption intensity, respectively.

The linear form of expression (4) is as follows (Parab et al., 2006):

$$Ln(q) = ln(K_F) + (1/n).ln(C_e) \quad (5)$$

This data were correlated according to Langmuir and Freundlich isotherms and the results are given in Table (1) and are graphically depicted in Fig. (12 a & b). The adsorption equilibrium analysis in figure shows that Freundlich and Langmuir models give fit to the adsorption isotherm in the investigated concentration range, in accordance with higher R^2 values for both Freundlich and Langmuir isotherms.

Such fitting may be related to the presence of variable adsorption sites on the surface of the nanoparticles, i.e. physical chemisorption and adsorption.

The values of the separation factor, R_L, in Table (1), are less than 1 and larger than 0 indicating favorable adsorption. This was confirmed with the values of Freundlich coefficient n being larger than one which in turn is indicative of physical adsorption.

Table 1. Results of Adsorption Equilibrium Analysis

Langmuir isotherm:					
K_L (L/mmol)		Q_m (mmol/g)		R^2	
28.64		0.0440		0.9902	
Freundlich isotherm:					
K_F		n		R^2	
0.0511		1.5499		0.9868	
C_0 (mmol/L)	0.16	0.31	0.47	0.62	0.78
R_L (Separation factor)	0.18	0.10	0.07	0.05	0.04

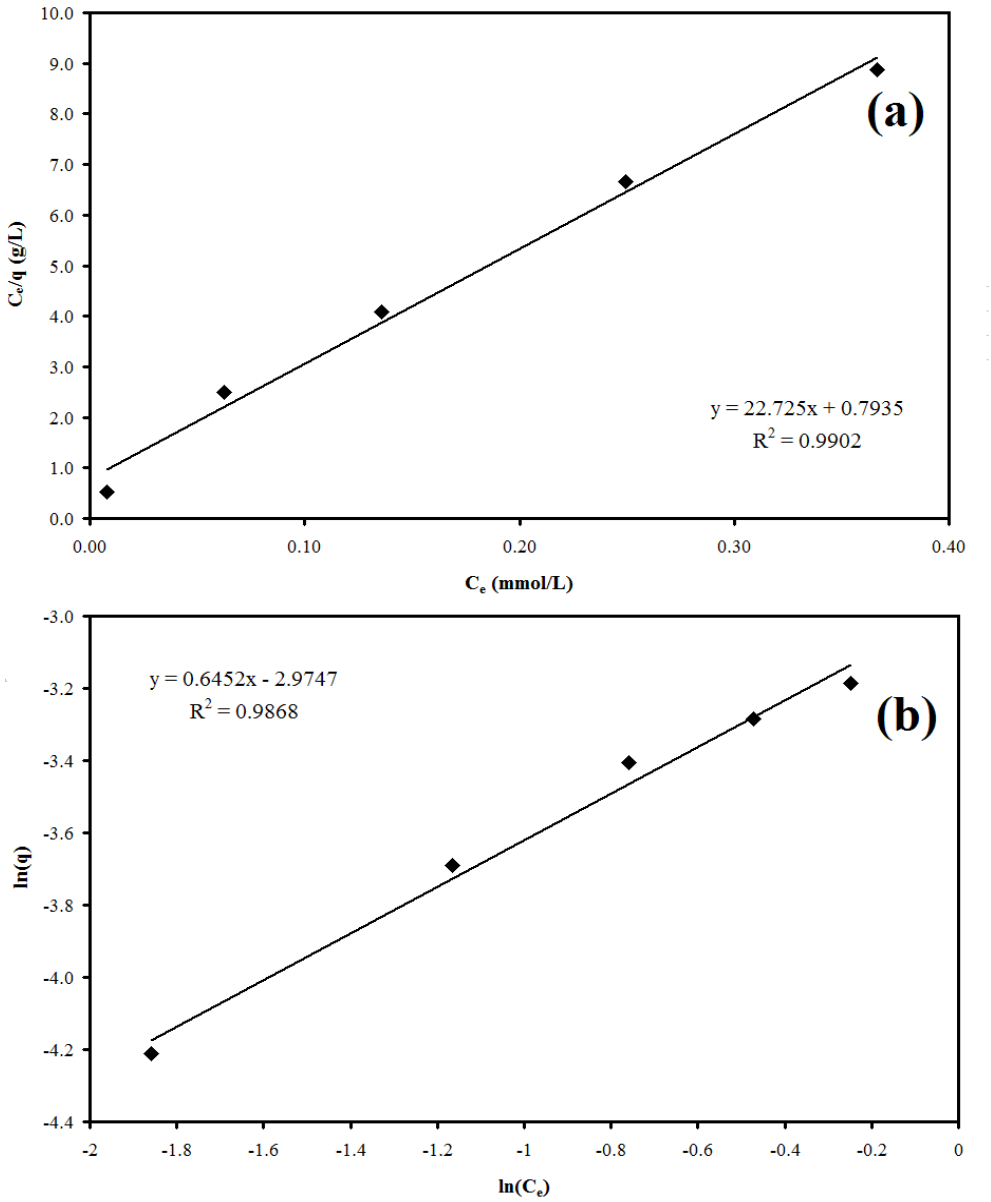

Figure 12. Results of equilibrium analysis: (a) Langmuir model and (b) Freundlich model.

The experimental (41.33 μmol/g Fig. 11) and calculated (44.00 μmol/g, Table 1) equilibrium data exhibited good agreement.

In order to gain a better understanding of the adsorption process the kinetic models are used to test the experimental data.

For this purpose pseudo-first order model, pseudo-second order model and intraparticle diffusion models were used (Muzic et al., 2010).

The pseudo-first order rate Lagergren model is:

$r_q = k_1 (q_e - q) = dq/dt$ (6)

where q (μmol/gm) is the amount of adsorbed DMDS on the adsorbent at time t (min), k_1 (min^{-1}) is the rate constant of the pseudo-first order adsorption and q_e (μmol/gm) is the equilibrium sorption uptake.

The integrated form of Eq. (6) is:

$\ln(q_e - q) = \ln(q_e) - k_1 t$ (7)

Linear plot of $\ln(q_e - q)$ versus t is used to determine $q_{e,\,cal}$ (which is calculated sorption capacity, μmol/gm) and k_1.

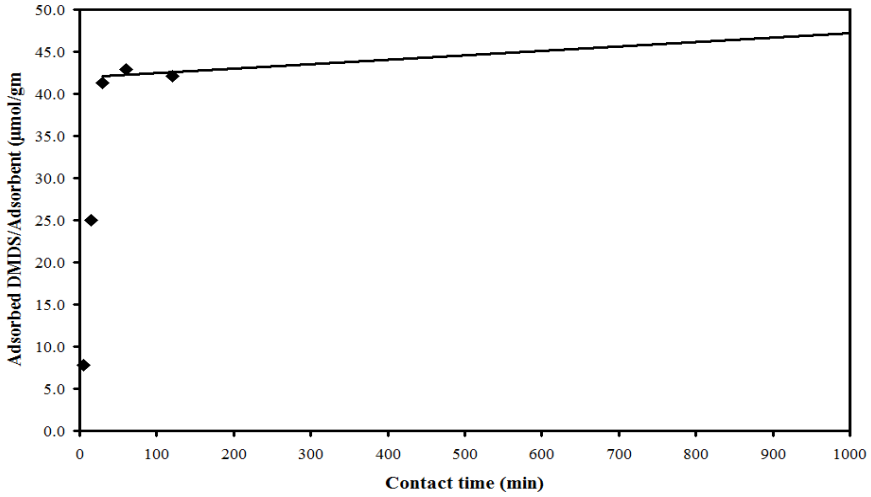

Figure 13. The relation between the specific adsorption and the contact time.

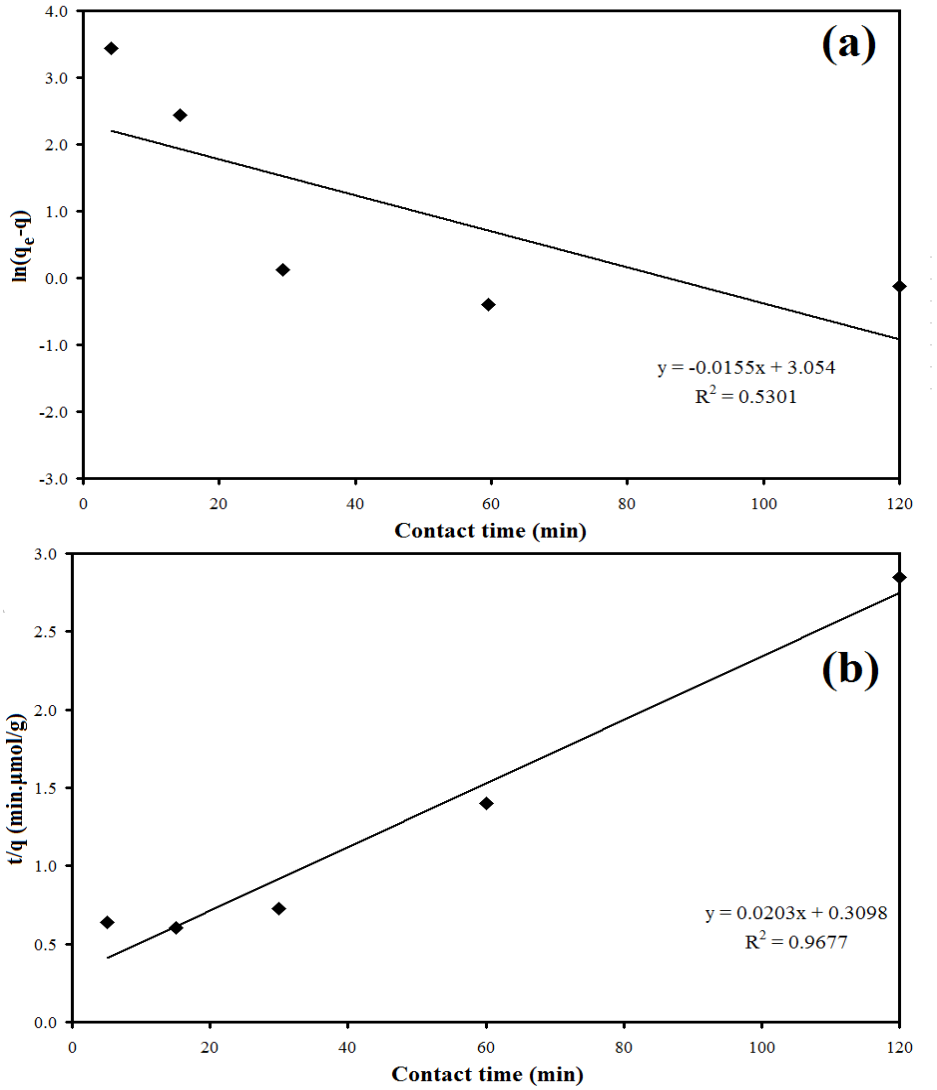

Figure 14. Results of kinetic analysis: (a) pseudo-first order model, and (b) pseudo-second order model.

In order to calculate the $\ln(q_e-q)$ values, the amount of adsorbed DMDS on the adsorbent was assumed to be 47.3 μmol/gm based on the hypothetical extrapolation of the equilibrium plateau in Fig (8) till contact time 1000 min (Fig. 13, Muzic et al., 2010).

The pseudo-second order rate model is:

$$r_q = k_2 (q_e-q)^2 = dq/dt \quad (8)$$

where k_2 (g/μmol. min) is the rate constant of pseudo-second order adsorption. The integrated form of Eq. (8) is:

$$t/q = 1/k_2q^2_e + (1/q_e)t \quad (9)$$

q_e and k_2 can be determined by plotting t/q versus t. It can be noticed that for the application of this model the value of q_e does not need to be estimated from the experimental data (Stoica et al., 2007).

The same is true for the intraparticle diffusion model (Wu, 2007) which is written as:

$$q = k_it^{(1/2)} + C \quad (10)$$

where k_i is the intraparticle diffusion rate constant (μmol/g.min$^{1/2}$) and C (μmol/g) is the constant related to the energy of adsorption. Intraparticle diffusion model constants can be determined as slope and intercept of the linear plot of q versus $t^{(1/2)}$, respectively.

The results of kinetic analysis are graphically presented in Fig. 14(a-b). Table (2) presents the results and the correlation coefficients of the pseudo-first and pseudo-second order adsorption kinetic models and intraparticle diffusion model.

Table 2. Results of Kinetic Analysis

pseudo-first order model		
$q_{e,\,cal}$ (μmol/g)	k_1 (min^{-1})	R^2
21.20	0.0105	0.5301
pseudo-second order model		
$q_{e,\,cal}$ (μmol/g)	k_2 (g/μmol.min)	R^2
49.26	0.0013	0.9677
intraparticle diffusion model		
C (μmol/g)	k_i (μmol/g.min$^{1/2}$)	R^2
9.6449	3.6601	0.6612

The equilibrium sorption uptake value calculated from pseudo-first order model differ substantially from hypothetical adsorption capacity after 1000 min while the $q_{e,\,cal}$ value attained from pseudo-second order model is only slightly higher. These results, alongside the facts that points on the graphic interpretation of pseudo-second order model (Fig. 14 (b)) lie on the straight line and the correlation coefficient, R^2, values is nearly equal to 1 are suggesting that kinetic of adsorptive desulfurization can be excellently described by the pseudo-second order model indicating that the adsorption of organic sulfur compounds closely follows the second order reaction path. However, the low value of pseudo-second order rate constant of tested adsorbent (0.0013 g/μmol.min) indicates that adsorptive desulfurization is a relatively slow process.

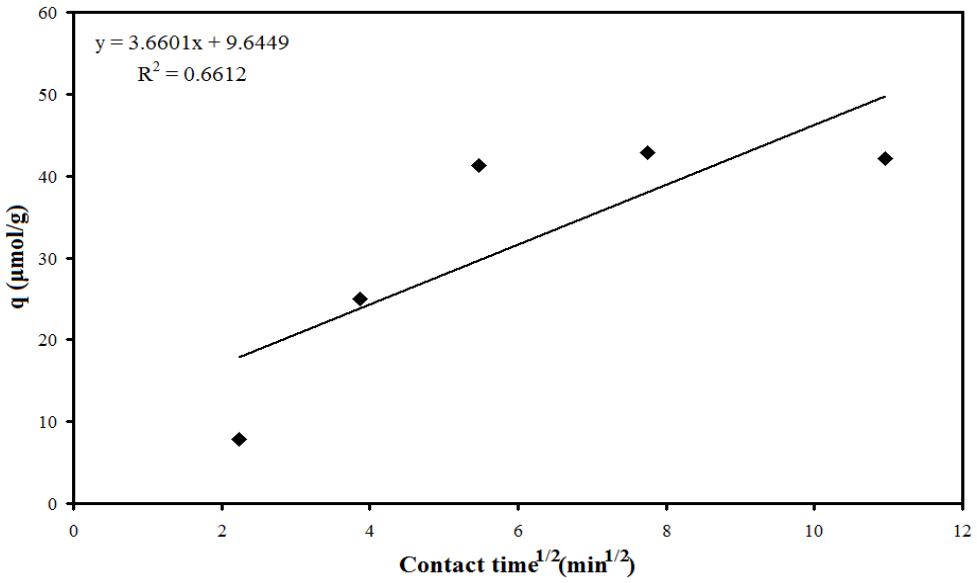

Figure 15. Results of kinetic analysis of intraparticle diffusion model.

Typically, various mechanisms control the adsorption kinetics; the most limiting are the diffusion mechanisms, including external diffusion, boundary layer diffusion and intraparticle diffusion (Guibal et al., 2003). Hence, the intraparticle diffusion model was utilized to determine the rate-limiting step of the adsorption process. If the regression of q versus $t^{1/2}$ is linear and passes through the origin, the intraparticle diffusion is the proper rate-limiting step (Ozcan and Ozcan, 2005; Kannan and Sundaram, 2001).

As it can be clearly seen in Fig. (15) the regression was not linear and it did not pass through the origin for the investigated adsorbent, suggesting that the adsorption is not influenced by the intraparticle diffusion and that it was not the rate controlling step.

4. Conclusion

The prepared MW2-1.5 exhibits the highest adsorption % as compared with the other samples. Such activity is attributed to the presence of the $Mo_{0.5}W_{0.5}O_3$ nanoparticles as conformed by XRD and TEM analyses. This situation creates and enlarges the amount of active fine sites which are able to remove the hetero sulfur atoms.

It is worth to suggest that the prepared crystalline nano-sized particles molybdenum-tungsten bimetallic oxides will find application as a guard bed adsorbent in the petroleum reformer to avoid catalyst deactivation and to improve the life of the hydrotreating catalyst. In other words, to get a product containing least amount of sulfur which is necessary for making an acceptable feed for reforming process.

References

Babich I.V., Moulijn J.A., (2003): Science and technology of novel processes for deep desulfurization of oil refinery streams: a review, Fuel, 82, 607-631.

El-Shobaky H. G., Mokhtar M., and Ahmed A. S., (1999): Effect of MgO-doping on solid-solid interactions in MoO_3/Al_2O_3 system, Thermochimica Acta, 327, 39–46.

Guibal E., McCarrick P. and Tobin J.M., (2003): Comparison of the sorption of anionic dyes on activated carbon and chitosan derivatives from dilute solutions. Sep Sci Technol, 38, 3049–3073.

Hassan H., Zaki T., Mikhail S., Kandil A., Farag A. (2012): Optimization of the Synthesis of Nanostructured Tungsten-Molybdenum Bimetallic Oxide. ISRN Nanomaterials, 2012, 1-13.

Kannan K. and Sundaram M., (2001) Kinetics and mechanism of removal of methylene blue bya dsorption on various carbons comparative study, Dyes Pigments, 51, 25–40.

Ma X., Velu S., Kim J.H., Song C., (2005): Deep desulfurization of gasoline by selective adsorption over solid adsorbents and impact of analytical methods on ppm-level sulfur quantification for fuel cell applications, Appl. Catal. B Environ., 56, 137-147.

Muzica M., Biondaa K., Gomzia Z., Podolskib S., Telenb S., (2010): Study of diesel fuel desulfurization by adsorption, Chemical Engineering Research and Design, 88, 487-495.

Ozcan, A. and Ozcan, A.S., (2005): Adsorption of Acid Red 57 from aqueous solutions onto surfactant-modified sepiolite J. Hazard Mater, 125, 252–259.

Parab H., Joshi S., Shenoy N., Lali A., Sarma U.S. and Sudersanan M., (2006): Determination of kinetic and equilibrium parameters of the batch adsorption of Co(II) Cr(III) and Ni(II) onto coir pith. Process Biochem, 41, 609–615.

Pechini M.P., (1967): US Pat., 3330697.

Prince R.C., Grossman M.J., (2003): Substrate Preferences in Biodesulfurization of Diesel Range Fuels by Rhodococcus sp. Strain ECRD-1, Appl. Environ. Microbiol., 69, 5833-5838.

Sarkar A., Pramanik S., Achariya A., and Pramanik P., (2008): A novel sol-gel synthesis of mesoporous ZrO_2-MoO_3/WO_3 mixed oxides, Microporous and Mesoporous Materials, 115, 426–431.

Shaheen W. M., (2002): Thermal solid-solid interaction and catalytic properties of CuO/Al_2O_3 system treated with ZnO and MoO_3, Thermochimica Acta, 385, 105–116.

Stoica A., Stroescu M., Iavorschi G. and Dobre T., (2007): Kinetic studies on methylene blue adsorption on various activated carbons, in Proc. of the 34th International Conference of SSCHE, Markos J. and Stefuca V. Stefuca V. (eds) SSCHE, Tatranske Matliare, Slovakia,

Te M., Fairbridge C., Ring Z., (2001): Oxidation reactivities of dibenzothiophenes in polyoxometalate/H_2O_2 and formic acid/H_2O_2 systems, Appl. Catal. A General, 219, 267-280.

Tolstoy V., Chernyshova I., and Skryshevsky V.,(2003): Handbook of Infrared Spectroscopy of Ultrathin Films, John Wiley & Sons, Hoboken, NJ, USA,.

US EPA Clean Air Act Tier 2, 1999.

Wang F., Li C., Jimmy C.,(2011): Hexagonal Tungsten Trioxide Nanorods as a Rapid Adsorbent for Methylene Blue, Separation and Purification Technology, 10,10-16.

Wang S., An Y., Zhang C., Zhang Z., Qian Y., (2006): Ethanothermal reduction to MoO_2 microspheres via modified Pechini method, J. Cryst. Growth 293, 209.

Whitehurst D.D., Isoda T., Mochida I., (1998): Present State of the Art and Future Challenges in the Hydrodesulfurization of Polyaromatic Sulfur Compounds, Adv. Catal., 42, 345-471.

Wu, C.H., (2007): Adsorption of reactive dye onto carbon nanotubes: equilibrium, kinetics and thermodynamics. J Hazard Mater, 144, 93–100.

Yu J., Qi L., Cheng B., and Zhao X., (2008): Effect of calcination temperatures on microstructures and photo catalytic activity of tungsten trioxide hollow microspheres, Journal of Hazardous Materials, 160, 621-628.

Zaki T., Khalid I. Kabel, H. Hassan, 2012, Preparation of high pure α-Al_2O_3 nanoparticles at low temperatures using Pechini method. Ceramics International 38, 2021–2026.

Zaki T., Khalid I. Kabel, H. Hassan, 2012, Using modified Pechini method to synthesize α-Al_2O_3 nanoparticles of high surface area. Ceramics International. 38 , 4861–4866

Zhu W., Li H., He X., Zhang Q., Shu H., and Yan Y., (2008): Synthesis of adipic acid catalyzed by surfactant-type peroxotungstates and peroxomolybdates, Catalysis Communications, 9, 551–555.

The IISTE is a pioneer in the Open-Access hosting service and academic event management. The aim of the firm is Accelerating Global Knowledge Sharing.

More information about the firm can be found on the homepage:
http://www.iiste.org

CALL FOR JOURNAL PAPERS

There are more than 30 peer-reviewed academic journals hosted under the hosting platform.

Prospective authors of journals can find the submission instruction on the following page: http://www.iiste.org/journals/ All the journals articles are available online to the readers all over the world without financial, legal, or technical barriers other than those inseparable from gaining access to the internet itself. Paper version of the journals is also available upon request of readers and authors.

MORE RESOURCES

Book publication information: http://www.iiste.org/book/

IISTE Knowledge Sharing Partners

EBSCO, Index Copernicus, Ulrich's Periodicals Directory, JournalTOCS, PKP Open Archives Harvester, Bielefeld Academic Search Engine, Elektronische Zeitschriftenbibliothek EZB, Open J-Gate, OCLC WorldCat, Universe Digtial Library , NewJour, Google Scholar